



# A comparison of two Stokes ice sheet models applied to the Marine Ice Sheet Model Intercomparison Project for plan view models (MISMIP3d)

Tong Zhang<sup>1,3</sup>, Stephen Price<sup>2</sup>, Lili Ju<sup>3</sup>, Wei Leng<sup>4</sup>, Julien Brondex<sup>5,6</sup>, Gaël Durand<sup>5,6</sup>, and Olivier Gagliardini<sup>5,6</sup>

<sup>1</sup>Institute of Climate System & Polar Meteorology, Chinese Academy of Meteorological Sciences, Beijing, China

<sup>2</sup>Fluid Dynamics and Solid Mechanics Group, Los Alamos National Laboratory, Los Alamos, NM, USA

<sup>3</sup>Department of Mathematics and Interdisciplinary Mathematics Institute, University of South Carolina, Columbia, SC, USA

<sup>4</sup>State Key Laboratory of Scientific and Engineering Computing, Chinese Academy of Sciences, Beijing, China

<sup>5</sup>CNRS, LGGE, 38041 Grenoble, France

<sup>6</sup>Université Grenoble Alpes, LGGE, 38041 Grenoble, France

Correspondence to: Stephen Price (sprice@lanl.gov)

## Abstract.

We present a comparison of the numerics and simulation results for two “full” Stokes ice sheet models, FELIX-S (Leng et al., 2012) and Elmer/Ice (Gagliardini et al., 2013). The models are applied to the Marine Ice Sheet Model Intercomparison Project for planview models (MISMIP3D). For the *diagnostic* experiment (P75D) the two models give very similar results (<2% difference with respect to along-flow velocities) when using identical geometries and computational meshes, which we interpret as an indication of inherent consistencies and similarities between the two models. For the *Stnd*, P75S, and P75R *prognostic* experiments, we find that FELIX-S (Elmer/Ice) grounding lines are relatively more retreated (advanced), results that are consistent with minor differences observed in the diagnostic experiment results and largely due to slightly different choices in the implementation of basal boundary conditions used by the two models. Based on current understanding, neither set of implementations is more or less favorable, in which case we propose that the span of different grounding line positions from these two models provides a measure of uncertainty when treating the results from full-Stokes models as a metric for accuracy in model intercomparison experiments. More importantly, we show that as grid resolution increases the grounding line positions for FELIX-S and Elmer/Ice appear to converge. We conclude that future model intercomparisons using full-Stokes models as a metric should include more than one model, to provide both additional confidence in the results from full-Stokes models and a measure of their uncertainty.

## 1 Introduction

As Earth’s largest reservoirs of fresh water, ice sheets are important components of the global climate system. Humans feel their impacts most acutely through changes in global sea level, as ice sheets grow or decay in response to climate forcing and internally controlled dynamics. While the rate of present-day sea-level rise is dominated by ocean steric changes and eustatic



changes due to shrinking mountain glaciers, the eustatic contribution from the large ice sheets (Greenland and Antarctica) has increased in recent decades and is expected to continue increasing in coming decades and centuries (Church and others, 2013; Clark et al., 2015). While currently smaller than the sea-level contribution from mountain glaciers or Greenland, the future sea-level rise contribution from Antarctica is of particular concern; because of inherent dynamic instabilities associated with marine-based ice sheets, the Intergovernmental Panel on Climate Change (IPCC) recently highlighted future Antarctic ice sheet evolution as the largest uncertainty with respect to projecting future rates of sea-level rise (Church and others, 2013).

Largely to address these concerns, the international community has focussed intense efforts over the last decade on improving the predictive skill of large-scale, whole-ice-sheet models. These improvements include increased fidelity and accuracy with respect to the governing nonlinear Stokes-flow equations, increased numerical and computational robustness and efficiency, increased complexity and realism with respect to representation of relevant physical processes, and increased efforts towards partial and full coupling with Earth System Models (e.g., see models described in Cornford et al. (2013); Favier et al. (2014); Seroussi et al. (2014); Feldmann and Levermann (2015); Tezaur et al. (2015)). Alongside and critical to advancing these efforts have been the development of model inter-comparison exercises, which have provided community-based “benchmark” solutions for gauging the correctness of model output (e.g., Pattyn et al., 2008, 2012, 2013). While designed to be simple, distilling a test for a particular model feature of interest down to its essence, these exercises are still generally too complicated for the application of formal model verification through the use of analytical or manufactured solutions. Thus, these same model intercomparisons have become increasingly dependent on the output from so-called “full” Stokes ice sheet models – the highest fidelity representation of the equations governing the momentum balance for ice flow – to provide a metric for the most accurate model solutions available. One example is the Elmer/Ice (Gagliardini et al., 2013), which has taken part in most of the intercomparison projects referenced above.

Here, we apply a second Stokes model, the FELIX-S model of Leng et al. (2012) (see also Leng et al., 2013, 2014; Zhang et al., 2015), to the Marine Ice Sheet Model Intercomparison for plan view models (MISMIP3d) experiments (Pattyn et al., 2013). We conduct a careful comparison of the numerical methods used, and the solutions produced by, FELIX-S and Elmer/Ice. Both models have undergone extensive formal verification (see Gagliardini et al., 2013; Leng et al., 2013) and have been shown to compare very favorably to one another when applied to the Ice Sheet Model Intercomparison for Higher-Order Models (ISMIP-HOM) (Pattyn et al., 2008) experiments (see, Figures 6, 7, 10, 11, 13, and 14 in Leng et al. (2012)). In a recent contribution, Gagliardini et al. (2016) show that both diagnostic and prognostic grounding line (GL) positions from Elmer/Ice exhibit substantial sensitivity as a function of not only the *across-flow* mesh resolution (*along-flow* mesh resolution has been explored and discussed in detail previously, e.g., Durand et al. (2009b)), but also as a function of seemingly arbitrary choices about how basal boundary conditions are implemented in the model. Here, by “arbitrary” we mean in the sense that it is not obvious if and why one choice should be superior to another. Below, we show that a similar level of sensitivity is apparent when comparing FELIX-S and Elmer/Ice output to marine ice sheet benchmark experiments, even when using the same computational mesh with very high along-flow resolution. While these differences clearly argue for a degree of caution when interpreting Stokes model output as the metric for model solution accuracy, we also show that the differences between Elmer/Ice and FELIX-S solutions decrease as the mesh resolution increases. The consistency between these two models at very



high resolution lends support for their use as a benchmark for lower fidelity models, provided these benchmark solutions are generated using adequate grid resolution.

The paper proceeds as follows. First, we give a brief overview of the governing Stokes-flow equations for ice flow, which are discretized and solved by Elmer/Ice and FELIX-S. We then discuss in some detail the implementation of boundary conditions – some specific to the problem of simulating marine ice sheets – and how they are implemented in the two models. A brief introduction to the MISMIP3d model setup is then given, followed by a presentation of experimental results for the two models. We then give an in-depth discussion of the similarities and differences between results from the two models, our interpretation of where these differences come from, and an assessment of their significance. We close with summary and concluding remarks.

## 2 Model Description

### 10 2.1 The Stokes ice flow model

Consider the flow of a viscous, incompressible fluid (ice) in a low-Reynolds number flow. Conservation of linear momentum is expressed by the balance between the stress-tensor divergence and the gravitational body force,

$$\nabla \cdot \boldsymbol{\sigma} = \rho_i \mathbf{g}, \quad (1)$$

with  $\boldsymbol{\sigma}$  representing the full stress tensor,  $\rho_i$  the density of ice, and  $\mathbf{g}$  the acceleration due to gravity.

15 The incompressibility of glacier ice is expressed as

$$\nabla \cdot \mathbf{u} = 0, \quad (2)$$

where  $\mathbf{u} = (u, v, w)$  denotes the ice velocity vector. For glacier ice, the constitutive relation can be expressed as for a Newtonian fluid,

$$\boldsymbol{\tau} = \boldsymbol{\sigma} + p\mathbf{I} = 2\eta\dot{\boldsymbol{\epsilon}}, \quad (3)$$

20 where  $\boldsymbol{\tau}$  is the deviatoric stress tensor,  $p$  is the isotropic ice pressure,  $\mathbf{I}$  is the identity tensor,  $\dot{\boldsymbol{\epsilon}}$  is the strain rate tensor, and  $\eta$  is the “effective” viscosity, defined by Nye’s generalization of Glen’s flow law (Cuffey and Paterson, 2010),

$$\eta = \frac{1}{2} A^{-1/n} \dot{\epsilon}_e^{(1-n)/n}. \quad (4)$$

The flow-law exponent  $n$  is assigned a value of 3, with  $n > 1$  leading to a “shear thinning”, non-linear rheology.  $A$  is the temperature-dependent rate factor and  $\dot{\epsilon}_e$  is the effective strain rate (the square root of the 2nd invariant of the strain-rate tensor).

### 2.2 Boundary conditions

At the upper surface, a stress-free boundary condition applies,

$$\boldsymbol{\sigma} \cdot \mathbf{n} = 0, \quad (5)$$



where  $\mathbf{n} = (\hat{x}, \hat{y}, \hat{z})$  is the surface normal vector in a Cartesian reference frame. The lower-ice surface consists of two different boundary conditions (Durand et al., 2009a). For the “grounded” part of the flow where ice is in contact with bedrock (i.e., the ice-bedrock interface), the normal stress exerted by the ice body is larger than ocean water pressure. Here we apply the non-linear friction sliding law prescribed for the MISMIP3d experiments (Pattyn et al., 2013),

$$5 \quad \sigma_{nt_i} + C |\mathbf{u}|^{m-1} \mathbf{u} \cdot \mathbf{t}_i = 0, \quad (6)$$

where  $C$  is a friction coefficient that is non-zero for grounded ice only,  $\mathbf{t}$  is the bedrock tangent vector, and  $m$  is a friction-law exponent. For the floating part of the flow, where ice is detached from the bedrock (i.e., the ice-ocean interface, or the ice-bedrock interface at minimal floatation), the normal stress exerted by the ice body is smaller than *or equivalent to* the ocean water pressure, we apply a stress balance condition; normal stress,  $\sigma_{nn}$ , is balanced by the pressure due to buoyancy,  $P_w$ ,

$$10 \quad -\sigma_{nn} = P_w = \rho_w g(z_w - z), \quad (7)$$

where  $z_w$  is the sea level. For the case of  $z(x, y) = b(x, y)$ , we also need to consider a “contact problem” (Durand et al., 2009a) to decide the actual location of the GL. We discuss the contact problem and its implementation in Elmer/Ice and FELIX in more detail below.

The evolution of both the upper and lower free surfaces are determined by a kinematic boundary condition,

$$15 \quad \frac{\partial z_i}{\partial t} + u \frac{\partial z_i}{\partial x} + v \frac{\partial z_i}{\partial y} = w + \dot{a}_i, \quad (8)$$

for  $i = s, b$  denoting the upper and lower surfaces, respectively, and  $\dot{a}_i$  representing the surface or basal mass balance.

Consistent with the MISMIP3d experimental setup, the horizontal velocity is set to  $u = 0 \text{ m a}^{-1}$  at the ice divide ( $x = 0 \text{ km}$ ) and free-slip conditions are applied at the two lateral boundaries ( $y = 0 \text{ km}$  and  $y = 100 \text{ km}$ ).

20 Values for all model constants and parameters, including those that specifically apply to the MISMIP3d experimental protocols, are noted in Table 1.

### 2.3 Lower-order approximations

Lower-order approximations to the “full” Stokes equations expressed above, such as the “shallow-ice approximation” (SIA; Hutter, 1983) and “shallow-shelf approximation” (SSA; Morland, 1987), come about via geometric scaling arguments. These arguments can be used to show that, for many locations on glaciers and ice sheets, specific velocity gradient terms in the strain-rate tensor expressions above contribute negligibly to the momentum balance. While omitting these terms leads to a significant reduction in the numerical complexity and computational cost involved in solving the momentum balance equations (see e.g., Dukowicz et al., 2010; Schoof and Hindmarsh, 2010), the resulting errors may lead to non-negligible differences in dynamically complex regions of the ice sheet, such as near GLs (Pattyn and Durand, 2013). For this reason, full Stokes models are assumed to provide a better measure of the most complete and accurate solution near GLs, against which solutions from lower-order approximations may be compared in order to assess their accuracy.



### 3 Comparison of Model Numerics

Both FELIX-S and Elmer/Ice discretize the Stokes-flow momentum balance equations using Finite Element Methods (FEM). Additional details (and references) for Elmer/Ice are given in Gagliardini and Zwinger (2008) and Gagliardini et al. (2013), and for FELIX-S in Leng et al. (2012, 2013, 2014). Here, we provide a summary of several important similarities and differences  
5 between the numerical implementations used by Elmer/Ice and FELIX-S, noting that we view the differences as arbitrary. That is, there are *not* clear arguments for why one choice is superior to another and, in that sense, we view both methods as equally valid.

The first significant difference between Elmer/Ice and FELIX-S is in the choice of finite elements; Elmer/Ice uses hexahedral elements with P1-P1 basis functions (linear in velocity and pressure) and “bubble” function stabilization, whereas FELIX-S  
10 uses tetrahedral, Taylor-Hood elements with P2-P1 basis functions (quadratic in velocity, linear in pressure). The second important difference is that Elmer/Ice and FELIX-S use slightly different “masking” schemes for identifying grounded versus floating regions of the lower surface; Elmer/Ice marks the nodes bounding each element whereas FELIX-S marks the element faces. The third important difference, which is a generic FEM implementation issue and not specific to the Stokes-flow problem, is in how the value of the basal friction coefficient,  $C$ , is applied at the Gaussian quadrature points. FELIX-S calculates the  
15 values of  $C$  at quadrature points directly (with the accuracy of integration increasing with the number of integration points), whereas Elmer/Ice interpolates the values of  $C$  at Gaussian quadrature points from nodal values (Gagliardini et al., 2016) (with the number of integration points needed for a given degree of accuracy determined by the order of the basis function).

In terms of similarities, Elmer/Ice and FELIX-S use the same scheme for evolving the free surfaces, based on an FEM discretization of the kinematic boundary equation (8) (Gagliardini et al., 2013). The two models also use nearly identical  
20 implementations of the contact problem. For FELIX-S, the ocean water buoyancy pressure is compared to the normal *stress* of the ice on the bed and for Elmer/Ice, the ocean water buoyancy pressure is first integrated and then compared to the normal *force* of the ice on the bed (Durand et al., 2009a). While both models solve the contact problem at nodes, the information is used slightly differently; Elmer/Ice uses it to decide if *nodes* in contact with the bed are floating or grounded whereas FELIX-S uses it to decide if nodes in contact with the bed constitute an *element face* that is floating or grounded. We return to the discussion  
25 of these different schemes and their impact on model output in Section 6.

Lastly, of the three potentially different ways for defining how the basal friction coefficient  $C$  varies over the area of a grounded-to-floating element – “Last Grounded” (LG), “Discontinuous” (DI), and “First Floating” (FF) (discussed in more detail in Gagliardini et al., 2016) – FELIX-S uses what amounts to the DI implementation (the  $C$  values are discontinuous across the GL) (Figure 1). However, because the values of  $C$  are intimately tied to the location of the GL, and because of  
30 the different masking schemes used to decide on grounded versus floating nodes (in Elmer/Ice) or elements (FELIX-S), a direct comparison based on the implementation of the friction coefficient is really only meaningful for the P75D (diagnostic) simulation. We also return to this discussion in more detail in Section 6.



## 4 Experimental Setup

We provide a brief review of the MISMIP3d experimental setup, referring the reader to Pattyn et al. (2013) for additional details. Three experiments are conducted and reported on; the “standard” prognostic experiment (Stnd), the prognostic, basal sliding perturbation experiment (P75S and P75R), and the diagnostic experiment (P75D). The Stnd experiment is similar to that conducted in the original, two-dimensional MISMIP experiment for flowline models (Pattyn et al., 2012), where steady-state ice sheet GL positions are examined for a uniform, downward sloping (non-retrograde) bed in the along-flow ( $x$ ) direction, with a uniform basal friction coefficient and uniform bed properties in the across-flow ( $y$ ) direction. The goal is to compare three-dimensional model results to those from the two-dimensional test case, for which analytic solutions are available (Schoof, 2007). The prognostic P75S experiment starts from the steady-state geometry of the Stnd experiment and introduces a two-dimensional, Gaussian perturbation (a slippery patch) to the basal sliding coefficient field,  $C(x,y)$ , which introduces changes to the model state (velocity and geometry fields). The ice sheet geometry and GL are then allowed to advance for 100 years. The P75R experiment, which starts from the final state of the ice sheet at the end of the P75S experiment, returns the  $C(x,y)$  field to its original, uniform distribution, inducing GL retreat. The model is then integrated forward in time for another 100 years. The P75D experiment compares the diagnostic model state when using the P75S geometry calculated by the Elmer/Ice model. Below, we first report on the comparison between Elmer/Ice and FELIX-S for the P75D experiment. We then follow with a comparison for the Stnd, P75S and P75R experiments.

## 5 Results

### 5.1 The diagnostic experiment, P75D

We first compare the two models for the diagnostic experiment, P75D (Figure 2). Both models use the same parameters (e.g.,  $A$ ,  $C$ , and  $m$ ; see also Table 1) and, despite the different element types discussed above, have identical nodal coordinates over the entire model domain. From Figure 2, it is clear that the three velocity components ( $u$ ,  $v$  and  $w$ ) for Elmer/Ice and FELIX-S are in very good agreement for both the upper and lower surfaces, an indication of inherent consistencies between the two models. For this experiment, the most direct comparison between Elmer/Ice and FELIX-S is afforded by the DI results as, prior to determining  $C$ , we directly interpolate the *nodal* basal boundary condition mask from the Elmer/Ice diagnostic solution onto the *element-face* mask used by FELIX-S. In general, for the horizontal velocity,  $u$ , the differences are relatively small over the entire model domain (<2%), relatively less near the ice divide and increase continuously from the GL to the ice shelf portion of the domain (Figure 3). For the  $v$  and  $w$  velocity components, we observe relatively larger discrepancies in the region of the GL (around km 535 – 555), but still very small differences (<5%) over the majority of the domain (Figure 3).

Despite efforts to make mesh, initial and boundary conditions, and parameter settings identical between the two models, several non-negligible differences discussed above are likely responsible for the small differences in velocities shown in Figure 3. The first likely cause for the small differences is the different boundary masking schemes; as noted above, FELIX-S marks the basal boundary faces in an element-wise manner versus the node-wise manner used by Elmer/Ice. To apply as similar as



possible boundary settings for the P75D test case, FELIX-S applies the nodal mask from Elmer/Ice when generating its own element-based mask; element faces in FELIX-S are marked as grounded only if all 3 nodes of a triangle are marked as grounded according to the Elmer/Ice mask. Otherwise, the elements are marked as floating (Figure 1) (We note that this is *not* the same criteria that is used by FELIX-S in the remainder of the experiments to determine the location of floating versus grounded ice, as discussed further below). This may lead to small differences when assembling the element stiffness matrices and the right hand side vectors (for the Dirichlet boundary conditions) as part of the FEM discretization of the Stokes system. Another likely cause for the minor velocity differences in the P75D experiment is the specification of the sliding coefficient  $C$  at Gauss quadrature points, as discussed above in Section 3. Finally, despite identical mesh coordinates, Elmer/Ice and FELIX-S use different element types, basis functions, and interpolation schemes as discussed above.

Overall, for the P75D experiment FELIX-S results in slightly larger horizontal velocities ( $u$ ) at the GL than does Elmer/Ice. As a result, FELIX-S exhibits a slightly (1%) larger ice flux through the GL than does Elmer/Ice. This systematic difference between the two models is likely a combination of the slightly different numerical choices discussed above. Again, as these choices appear arbitrary with respect to our current level of understanding, it is not clear that the implementation and results from one model can be distinguished as being superior to the other.

## 5.2 Stnd prognostic experiment

The comparison of Elmer/Ice and FELIX-S diagnostic experiment results demonstrate that model solutions are very close to one another when using identical meshes, but that slightly different numerics and/or implementations of boundary conditions result in non-zero differences in the model solutions. In turn, the prognostic experiments demonstrate how those biases accumulate and affect the time-integrated model solutions.

For the Stnd prognostic experiment, FELIX-S uses the same initial ice sheet geometry and the same along- and across-flow resolution (50 and 2500 m, respectively) and mesh coordinates as Elmer/Ice. Both models demonstrate a continuous advance of the GL, with FELIX-S reaching a steady state GL position ( $x_g$ ) of 519.85 km (Table 2) and Elmer/Ice reaching steady state positions of  $x_g = 529.55, 526.80$  and  $522.35$  km, for LG, DI and FF, respectively (Gagliardini et al., 2016). Apparently, FELIX-S produces a slightly smaller equilibrium-sized ice sheet with a GL position that is slightly more retreated than that of Elmer/Ice.

We attribute the different equilibrium GL locations to differences in the numerical schemes already discussed above. While the overall retreated grounding line of FELIX-S relative to Elmer/Ice is consistent with the minor velocity differences observed – FELIX-S produces slightly higher along-flow velocities (and hence flux) upstream from, at, and downstream from the GL, with the time-integrated result of slightly thinner ice (and hence floatation) occurring slightly farther inland relative to Elmer/Ice – we note that Elmer/Ice velocities when using the FF scheme are significantly faster than for FELIX-S (Figures 1 and 2), and yet the Elmer/Ice GL when using the FF scheme is still advanced relative to that of FELIX-S (Table 2). Hence, other differences in the two numerical schemes must be more important in contributing to the observed steady-state GL location differences. We return to the discussion of these differences in greater detail in Section 6.



We repeated the Stnd prognostic experiment but starting from an initially over-sized configuration, allowing the ice sheet to shrink over time and the GL to retreat to its equilibrium position (as opposed to starting from an under-sized initial configuration with an advancing GL). In this case, we found  $x_g = 524.50$  km, approximately a 5 km difference relative to the case with an advancing GL. This difference is consistent with those found by Gagliardini et al. (2016) for their similar set of “MISMIP-3a” experiments (see their Figure 1c). We also expect that the steady-state GL locations from an advanced or retreated initial condition would ultimately converge with increasing grid resolution, as demonstrated in Gagliardini et al. (2016). This hypothesis is supported by the results of the P75S and P75R experiments, which we discuss next.

### 5.3 P75S and P75R prognostic experiments

In the P75S and P75R prognostic experiments, we investigate advance and retreat of the GL following a step-change perturbation in the basal friction distribution, for 100 years, and a return to the initial basal friction distribution, for a further 100 years (the “S” and “R” experiments, respectively), as discussed above in Section 4. The initial condition for the “S” experiment is the steady-state GL position of the Stnd prognostic experiment discussed above. To manage computational costs, especially in experiments where sensitivity to mesh resolution is explored, both models employ regional refinement near the GL. Initial mesh resolution in this region is 50 m along flow and 2500 m across flow for both models but, because of the different equilibrium GL positions for the Stnd experiment, FELIX-S and Elmer/Ice have slightly different refined meshes and thus have slightly different nodal coordinates for this set of experiments (i.e., the two model meshes are not identical as for the P75D and Stnd experiments).

Similar to the Stnd experiment, FELIX-S predicts relatively less GL advance (P75S) and / or relatively more GL retreat (P75R) than Elmer/Ice, as shown in Figures 4–6. Similar to Elmer/Ice (Gagliardini et al., 2016), FELIX-S shows a clear sensitivity to the *across-flow* resolution ( $\Delta y$ ); as the number of elements in the  $y$  direction increases from 20 to 80 ( $\Delta y$  decreases from 2500 m to 625 m), the “reversibility” – i.e. the return to the initial position – of the GL improves (Figures 4–6). Further, we also find that as the number of elements in the  $y$  direction increases from 20 to 80, the agreement between FELIX-S and Elmer/Ice increases for *all* of Elmer/Ice GL implementations (i.e., LG, DI, and FF; Figures 4–6).

## 6 Discussion

As noted above, some fraction of the differences in the prognostic model simulation results can likely be attributed to the small differences in the model velocity fields, as seen in the P75D experiment. In turn, these differences are likely related to the different type of finite elements and basis functions used by the two models. However, we attribute the bulk of the prognostic model simulation differences to differences in the treatment of the contact problem, and more importantly, to the different masking schemes used for the basal boundary conditions.

There are small differences in the way the contact problem is implemented in FELIX-S versus Elmer/Ice; while following the same physical basis for the contact problem, FELIX-S compares the normal stress and the sea water pressure acting at nodes, whereas Elmer/Ice compares the normal and sea water force acting at nodes (Durand et al., 2009a). The result may



be that, effectively, Elmer/Ice and FELIX-S “feel” slightly different normal forces (or pressures) at basal nodes of the ice-bed interface, resulting in slight differences when assessing whether a node (Elmer/Ice) or element (FELIX-S) is grounded or not. Unfortunately, the different element types used by FELIX-S and Elmer/Ice do not allow for a definitive confirmation of this hypothesis.

5 Of greater importance, however, are the different treatments of the basal boundary condition masking schemes discussed in Section 3. Figure 1 provides a schematic summary of the differences in the Elmer/Ice and FELIX-S basal boundary masking schemes and demonstrates how those differences would impact the GL location in the two models for a particular “edge” case. In the upper part of Figure 1, the nodes marked A and C are unambiguously floating (i.e.,  $z(x, y, t) > b(x, y)$ ), so that no contact problem needs to be considered for those nodes). Because FELIX-S considers any element with a floating node to be floating,  
10 elements 3, 4, and 8 are marked as floating, with the resulting FELIX-S GL position shown by the blue line in Figure 1. For the same geometric configuration, the node-based scheme used by Elmer/Ice defines a slightly different position for the GL, shown by the red line in Figure 1.

In addition to the slightly different grounding line locations, the different basal boundary masking schemes will lead to different profiles for  $C$ , as shown schematically in the lower part of Figure 1 where we plot approximate nodal  $C$  profiles for  
15 the two models. These differences come about because, for FELIX-S, the nodal matrix coefficients contain the contributions of  $C$  (and other variables) from the surrounding elements. As an example, consider profiles 1 and 3 in Figure 1. The  $C = 0$  contributions from elements 3 and 8, and assuming additional floating elements to the north of element 3 and to the south of element 8, reduce the matrix coefficients associated with the node along the centers of profiles 1 and 3 by a factor of approximately  $2/6=1/3$  (for these nodes, 2 of the 6 surrounding elements are floating), relative to Elmer/Ice. This estimate is  
20 only approximate because, in reality, the nodal coefficients contain additional terms related to the ice velocity and the basis functions, which are not uniform for all elements surrounding a node. Similarly, assuming that additional elements downstream of the FELIX-S GL are also floating, the coefficient at node B along profile 2 will be reduced by  $\sim 5/6$  relative to the Elmer/Ice value, since 5 of the 6 surrounding elements are floating.

We attribute the majority of the differences observed in prognostic model simulations to these slight differences in GL  
25 position, and more importantly to these slight differences in the value of  $C$ . If we again consider profile 2 in Figure 1 (and to a lesser extent profiles 1 and 3), the relatively larger value of  $C$  for Elmer/Ice will lead to relatively less basal sliding there and, eventually, relatively thicker ice. This in turn will result in a higher likelihood that neighboring nodes may also eventually ground. The overall, time-integrated result will be that, all other things being equal, the Elmer/Ice masking scheme will slightly favor grounding and/or grounding line advance relative to the FELIX-S scheme. This proposed difference in model behavior  
30 is consistent with the differences observed when the two models are applied to the prognostic experiments.

We further note that the differences between the nodal  $C$  profiles for Elmer/Ice and FELIX-S shown in Figure 1 are broadly similar to the differences between the DI and FF implementations in Elmer/Ice; despite the DI-like implementation of  $C$  in FELIX-S, the different masking scheme results in  $C$  values at nodes that effectively “look” more similar to the FF implementation of Elmer/Ice (dashed  $C$  profile lines in Figure 1). Simulations using Elmer/Ice with these two different implementation  
35 demonstrate differences that are broadly similar to the FELIX-S and Elmer/Ice differences observed here for prognostic sim-



ulations; the FELIX-S equilibrium grounding line for the Stnd experiment is closest to that for Elmer/Ice when using the FF implementation (Table 2), the change in FELIX-S GL in the P75S experiment is closest to that observed for Elmer/Ice when using the FF implementation (Table 2), and, at all across-flow resolutions, the advance and retreat curves for FELIX-S in the P75S and P75R experiments most closely resemble those for Elmer/Ice when using FF (Figures 4–6).

5 Based on our understanding of these model-to-model differences and their hypothesized impact on model simulations, we have a strong expectation that the differences in model outputs will decrease as model resolution increases. As the element size decreases, the gradients in ice sheet geometry that are the primary cause for differences in the nodal- versus element-based masking schemes will also decrease, and the two sets of model results should converge. Indeed this is exactly what we see for the P75S and P75R experiments. Similar to the observation of Gagliardini et al. (2016) that the LG, DI, and FF implementations  
10 in Elmer/Ice all converge to a similar solution with increasing resolution, we demonstrate here that the FELIX-S results also appear to converge to that same solution with increasing grid resolution (Figures 4-7).

## 7 Conclusions

We have conducted a first, detailed comparison of two full-Stokes ice sheet models, FELIX-S and Elmer/Ice, applied to the MIS3d benchmark experiments. While previous informal comparisons have suggested very close agreement between the  
15 two models (Leng et al., 2012), here we explore the model similarities and differences much more carefully, focussing on how differences in model numerics lead to differences in model outputs when using identical meshes and forcing.

Overall, we find very close agreement between the two model outputs for cases where the impact of rather arbitrary choices in the implementation of basal boundary conditions can be minimized; for the P75D experiment, diagnostic solutions (e.g., velocity fields) agree to within ~2-5%. While it is difficult to attribute those small differences to particular numerical choices  
20 made by the two models, it is likely that different element types and basis functions and slightly different implementations of the contact problem for floating ice play a role. More significant differences between the two sets of model results are found for prognostic problems. Overall, we find that equilibrium grounding lines for FELIX-S are relatively more retreated than those for Elmer/Ice (as demonstrated by the Stnd experiment) and that FELIX-S is slightly less inclined to ground, and hence less inclined to show grounding line advance than Elmer/Ice (as demonstrated by the Stnd and P75S and P75R experiments).

25 A detailed look at the two models strongly argues that differences in the basal boundary masking schemes and in the implementation of the basal friction coefficient is at the source of these differences. As we are currently unable to judge whether or not one scheme is superior to the other, our results urge caution when interpreting the results from full-Stokes as the metric for accuracy in model intercomparisons. More importantly, however, we are encouraged to find that, as the grid resolution for both models increases, the differences between the two models continues to decrease. This finding suggests (but  
30 does not prove) that, in the limit of high grid resolution, multiple full-Stokes models can be shown to agree on a particular test case solution, despite small differences in their numerics.

For these reasons, we propose that before full-Stokes model results are treated as an accuracy metric in future model inter-comparison exercises, two or more full-Stokes models should first conduct their own intercomparison, in order to more fully



explore the range of uncertainty associated with their solutions. As an example, the range of different grounding line trajectories for Elmer/Ice and FELIX-S shown here in Figure 6 might be interpreted as a range of uncertainty when gauging the results of lower-order models against those from Stokes models for the P75S and P75R experiments.

Future efforts could improve on the work presented here by allowing for a more direct comparison between models. This would include the use of identical element types and basis functions, identical basal boundary masking schemes, and identical implementations of the basal friction coefficient. While limited here by available computational resources, future efforts could also improve on the current work by running simulations at even finer grid resolutions, in order to definitively confirm that the results from multiple Stokes models converge in the limit of very fine grid resolution.

*Author contributions.* TZ and SP initiated the study with input from OG, GD, and JB. Necessary modifications to the FELIX-S model were made by TZ with input and guidance from original code authors LJ and WL. TZ conducted the FELIX-S simulations. JB, OG, and GD conducted Elmer/Ice simulations, provided results for comparison with FELIX-S, and provided insight when attributing simulation differences to model differences. TZ and SP wrote the paper with contributions from all co-authors.

*Acknowledgements.* The authors thank Frank Pattyn for initial discussions that helped to inspire and motivate this study. Support for TZ, SP, LJ, and WL was provided through the Scientific Discovery through Advanced Computing (SciDAC) program funded by the U.S. Department of Energy (DOE), Office of Science, Advanced Scientific Computing Research and Biological and Environmental Research. TZ was also supported by the National Basic Research Program (973) of China under grant No. 2013CBA01804. LJ was partially supported by the US National Science Foundation under grant No. DMS-1215659. WL was partially supported by the National 863 Project of China under grant No. 2012AA01A309 and the National Center for Mathematics and Interdisciplinary Sciences of the Chinese Academy of Sciences. Elmer/Ice development and simulations presented here were partly funded by the Agence Nationale pour la Recherche (ANR) through the SUMER, Blanc SIMI 6-2012. FELIX-S simulations presented here used computing resources of the National Energy Research Scientific Computing Center (NERSC; supported by the Office of Science of the U.S. Department of Energy under Contract DE-AC02-05CH11231). Elmer/Ice simulations discussed in this paper used computing resources of CINES (Centre Informatique National de l'Enseignement Supérieur, France) under allocations 2015-016066 made by GENCI (Grand Equipement National de Calcul Intensif).



## References

- Church, J. A. et al.: 2013: Sea Level Change. In: Climate Change 2013: The Physical Science Basis. Contribution of Working Group I to the Fifth Assessment Report of the Intergovernmental Panel on Climate Change [Stocker, T.F., D. Qin, G.-K. Plattner, M. Tignor, S.K. Allen, J. Boschung, A. Nauels, Y. Xia, V. Bex and P.M. Midgley (eds.)], Intergovernmental Panel on Climate Change, Working Group I Contribution to the IPCC Fifth Assessment Report (AR5)(Cambridge University Press, Cambridge, United Kingdom and New York, NY, USA.), 2013.
- Clark, P. U., Church, J. A., Gregory, J. M., and PAYNE, A. J.: Recent Progress in Understanding and Projecting Regional and Global Mean Sea Level Change, *Current Climate Change Reports*, 1, 224–246, 2015.
- Cornford, S. L., Martin, D. F., Graves, D. T., Ranken, D. F., Brocq, A. M. L., Gladstone, R. M., Payne, A. J., Ng, E. G., and Lipscomb, W. H.: Adaptive mesh, finite volume modeling of marine ice sheets, *Journal of Computational Physics*, 232, 529 – 549, doi:http://dx.doi.org/10.1016/j.jcp.2012.08.037, 2013.
- Cuffey, K. and Paterson, W.: *The Physics of Glaciers*, Elsevier, Amsterdam, 4<sup>th</sup> edn., 2010.
- Dukowicz, J. K., Price, S. F., and Lipscomb, W. H.: Consistent approximations and boundary conditions for ice-sheet dynamics from a principle of least action, *J. Glaciol.*, 56, 480–496, doi:10.3189/002214310792447851, 2010.
- 15 Durand, G., Gagliardini, O., de Fleurian, B., Zwinger, T., and Le Meur, E.: Marine ice sheet dynamics: Hysteresis and neutral equilibrium, *J. Geophys. Res.*, 114, F03 009, doi:10.1029/2008JF001170, 2009a.
- Durand, G., Gagliardini, O., Zwinger, T., Le Meur, E., and Hindmarsh, R. C. A.: Full Stokes modeling of marine ice sheets : influence of the grid size, *Ann. Glaciol.*, 50, 109–114, 2009b.
- Favier, L., Durand, G., Cornford, S. L., Gudmundsson, G. H., Gagliardini, O., Gillet-Chaulet, F., Zwinger, T., Payne, a. J., and Le Brocq, a. M.: Retreat of Pine Island Glacier controlled by marine ice-sheet instability, *Nat. Clim. Chang.*, 5, 117–121, doi:10.1038/nclimate2094, 2014.
- 20 Feldmann, J. and Levermann, A.: Collapse of the West Antarctic Ice Sheet after local destabilization of the Amundsen Basin, *Proceedings of the National Academy of Sciences*, 112, 14 191–14 196, doi:10.1073/pnas.1512482112, 2015.
- Gagliardini, O. and Zwinger, T.: The ISMIP-HOM benchmark experiments performed using the Finite-Element code Elmer, *Cryosph.*, 2, 67–76, 2008.
- 25 Gagliardini, O., Zwinger, T., Gillet-Chaulet, F., Durand, G., Favier, L., de Fleurian, B., Greve, R., Malinen, M., Martín, C., Rå back, P., Ruokolainen, J., Sacchetti, M., Schäfer, M., Seddik, H., and Thies, J.: Capabilities and performance of Elmer/Ice, a new-generation ice sheet model, *Geosci. Model Dev.*, 6, 1299–1318, doi:10.5194/gmd-6-1299-2013, 2013.
- Gagliardini, O., Brondex, J., Gillet-Chaulet, F., Tavard, L., Peyaud, V., and Durand, G.: Brief communication: Impact of mesh resolution for MISMIP and MISMIP3d experiments using Elmer/Ice, *The Cryosphere*, 10, 307–312, doi:10.5194/tc-10-307-2016, 2016.
- 30 Hutter, K.: *Theoretical Glaciology: Material Science of Ice and the Mechanics of Glaciers and Ice Sheets*, Reidel, Dordrecht, 1983.
- Leng, W., Ju, L., Gunzburger, M., Price, S., and Ringler, T.: A Parallel High-Order Accurate Finite Element Nonlinear Stokes Ice Sheet Model and Benchmark Experiments, *J. Geophys. Res.*, 117, 2156–2202, doi:10.1029/2011JF001962, 2012.
- Leng, W., Ju, L., Gunzburger, M., and Price, S.: Manufactured solutions and the verification of three-dimensional Stokes ice-sheet models, *Cryosph.*, 7, 19–29, doi:10.5194/tc-7-19-2013, 2013.
- 35 Leng, W., Ju, L., Gunzburger, M., and Price, S.: A parallel computational model for three-dimensional, thermo-mechanical Stokes flow simulations of glaciers and ice sheets, *Comm. Comput. Phys.*, pp. 1056–1080, doi:10.4208/cicp.310813.010414a, 2014.



- Morland, L.: Unconfined ice-shelf flow, in *Dynamics of the West Antarctic Ice Sheet*, Reidel, Dordrecht, 1987.
- Pattyn, F. and Durand, G.: Why marine ice sheet model predictions may diverge in estimating future sea level rise, *Geophysical Research Letters*, 40, doi:10.1002/grl.50824, 2013.
- Pattyn, F., Perichon, L., Aschwanden, a., Breuer, B., de Smedt, B., Gagliardini, O., Gudmundsson, G. H., Hindmarsh, R. C. a., Hubbard, a.,  
5 Johnson, J. V., Kleiner, T., Konovalov, Y., Martin, C., Payne, a. J., Pollard, D., Price, S., Rückamp, M., Saito, F., Souček, O., Sugiyama, S., and Zwinger, T.: Benchmark experiments for higher-order and full-Stokes ice sheet models (ISMIP-HOM), *Cryosph.*, 2, 95–108, doi:10.5194/tc-2-95-2008, 2008.
- Pattyn, F., Schoof, C., Perichon, L., Hindmarsh, R. C. a., Bueler, E., de Fleurian, B., Durand, G., Gagliardini, O., Gladstone, R., Goldberg, D., Gudmundsson, G. H., Huybrechts, P., Lee, V., Nick, F. M., Payne, a. J., Pollard, D., Rybak, O., Saito, F., and Vieli, a.: Results of the  
10 Marine Ice Sheet Model Intercomparison Project, MISMIP, *Cryosph.*, 6, 573–588, doi:10.5194/tc-6-573-2012, 2012.
- Pattyn, F., Perichon, L., Durand, G., Favier, L., Gagliardini, O., Hindmarsh, R. C., Zwinger, T., Albrecht, T., Cornford, S., Docquier, D., Fürst, J. J., Goldberg, D., Gudmundsson, G. H., Humbert, A., Hütten, M., Huybrechts, P., Jouvét, G., Kleiner, T., Larour, E., Martin, D., Morlighem, M., Payne, A. J., Pollard, D., Rückamp, M., Rybak, O., Seroussi, H., Thoma, M., and Wilkens, N.: Grounding-line migration in plan-view marine ice-sheet models: results of the ice2sea MISMIP3d intercomparison, *J. Glaciol.*, 59, 410–422,  
15 doi:10.3189/2013JoG12J129, 2013.
- Schoof, C.: Ice sheet grounding line dynamics: Steady states, stability, and hysteresis, *J. Geophys. Res.*, 112, F03S28, doi:10.1029/2006JF000664, 2007.
- Schoof, C. and Hindmarsh, R. C. A.: Thin-Film Flows with Wall Slip: An Asymptotic Analysis of Higher Order Glacier Flow Models, *The Quarterly Journal of Mechanics and Applied Mathematics*, 63, 73–114, 2010.
- 20 Seroussi, H., Morlighem, M., Larour, E., Rignot, E., and Khazendar, a.: Hydrostatic grounding line parameterization in ice sheet models, *Cryosph. Discuss.*, 8, 3335–3365, doi:10.5194/tcd-8-3335-2014, 2014.
- Tezaur, I. K., Perego, M., Salinger, a. G., Tuminaro, R. S., and Price, S. F.: Albany/FELIX: a parallel, scalable and robust, finite element, first-order Stokes approximation ice sheet solver built for advanced analysis, *Geosci. Model Dev.*, 8, 1197–1220, doi:10.5194/gmd-8-1197-2015, 2015.
- 25 Zhang, T., Ju, L., Leng, W., Price, S., and Gunzburger, M.: Thermomechanically coupled modelling for land-terminating glaciers: a comparison of two-dimensional, first-order and three-dimensional, full-Stokes approaches, *J. Glaciol.*, 61, 702–712, doi:10.3189/2015JoG14J220, 2015.

## Tables and figures



**Table 1.** Parameters used in Elmer/Ice and FELIX-S.

Symbol	Constant	Value/Units
$\rho_i$	ice density	900 kg m <sup>-3</sup>
$\rho_w$	water density	1000 kg m <sup>-3</sup>
$g$	gravitational acceleration	9.8 m s <sup>-2</sup>
$n$	flow law exponent	3
$A$	flow law parameter	10 <sup>-25</sup> s <sup>-1</sup> Pa <sup>-3</sup>
$C$	Bed friction parameter	10 <sup>7</sup> Pa m <sup>-1/3</sup> s <sup>1/3</sup>
$m$	Bed friction exponent	1/3
$\dot{a}_s$	Accumulation rate	0.5 m a <sup>-1</sup>

**Table 2.** Comparison between Elmer/Ice (LG, DI and FF) and FELIX-S GL positions for the Stnd and P75S experiments. The  $x_{G_0}$  denotes the steady state GL position in the Stnd experiment. The rows for  $\Delta x_{GLc}$  and  $\Delta x_{GLm}$  denote the differences between  $x_{G_0}$  and the GL position at year 100 in the P75S experiment, at the centerline and margin, respectively.

	FELIX-S			Elmer/Ice (LG)			Elmer/Ice (DI)			Elmer/Ice (FF)		
	20	40	80	20	40	80	20	40	80	20	40	80
$N_y$	20	40	80	20	40	80	20	40	80	20	40	80
$x_{G_0}$	519.850	–	–	529.550	–	–	526.800	–	–	522.350	–	–
$\Delta x_{GLc}$	0.100	4.350	9.400	18.950	16.350	15.050	9.250	10.825	11.950	1.950	6.425	9.900
$\Delta x_{GLm}$	–14.050	–8.950	–6.250	–0.100	–2.750	–3.850	–8.000	–7.050	–6.250	–13.050	–10.250	–7.850

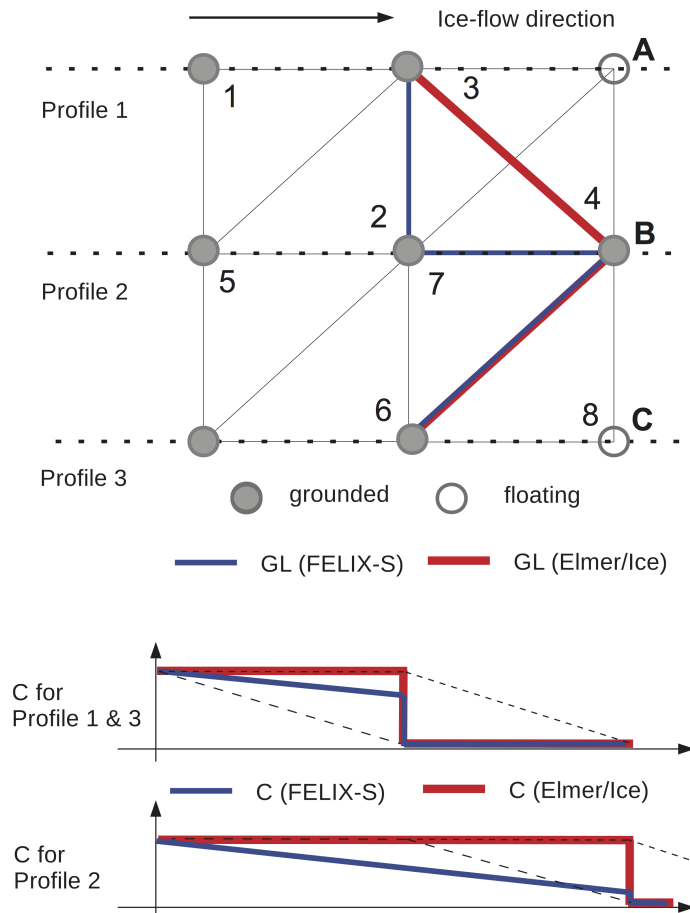


**Figure 1.** A schematic of the different basal boundary masking schemes used by FELIX-S and Elmer/Ice and their impact on the definition of the MISIP3d basal friction coefficient ( $C(x, y) = C$  for grounded ice and  $C(x, y) = 0$  for floating ice). Circles denote the nodes at the ice-bed interface, defining the basal finite element faces (triangular and quadrilateral for FELIX-S and Elmer/Ice, respectively); open circles denote floating nodes for which  $z(x, y, t) > b(x, y)$  and solid circles denote grounded nodes for which  $z(x, y, t) = b(x, y)$  and  $-\sigma_{nn} > P_w$ . Numbers 1-8 identify triangular elements of FELIX-S and letters A-C identify specific nodes common to both models. As discussed in Section 6, the different masking schemes lead to the different grounding line positions and also to the different nodal values of  $C$  along profiles 1-3. The  $C$  profiles based on DI for Elmer/Ice (heavy red line) and FELIX-S profiles (heavy blue line) are shown, as are the corresponding Elmer/Ice FF (black dashed) and LG (black dotted) profiles.

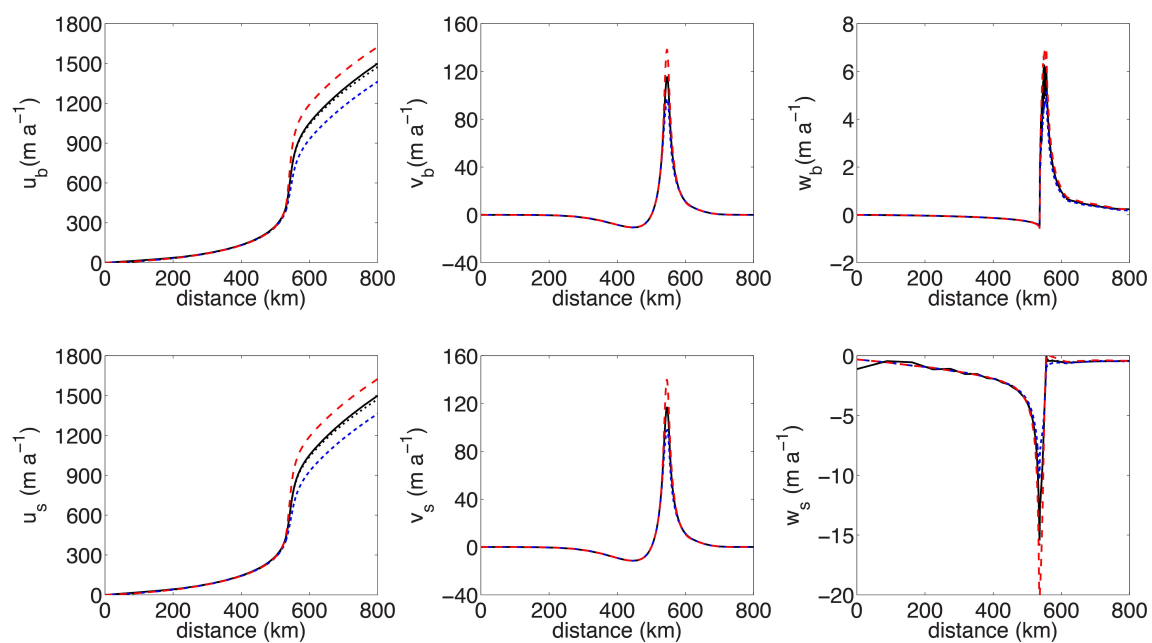


**Figure 2.** Comparisons of mean across-flow velocities for lower ( $u_b$ ,  $v_b$ ,  $w_b$ ) and upper ( $u_s$ ,  $v_s$  and  $w_s$ ) surfaces along the  $x$  direction for FELIX-S (black-solid line), Elmer/Ice FF (red-dashed line), DI (black-dotted line) and LG (blue-dotted line) cases for the diagnostic experiment P75D. Where the black dotted line is not clearly visible, Elmer/Ice and FELIX-S solutions are overlying.

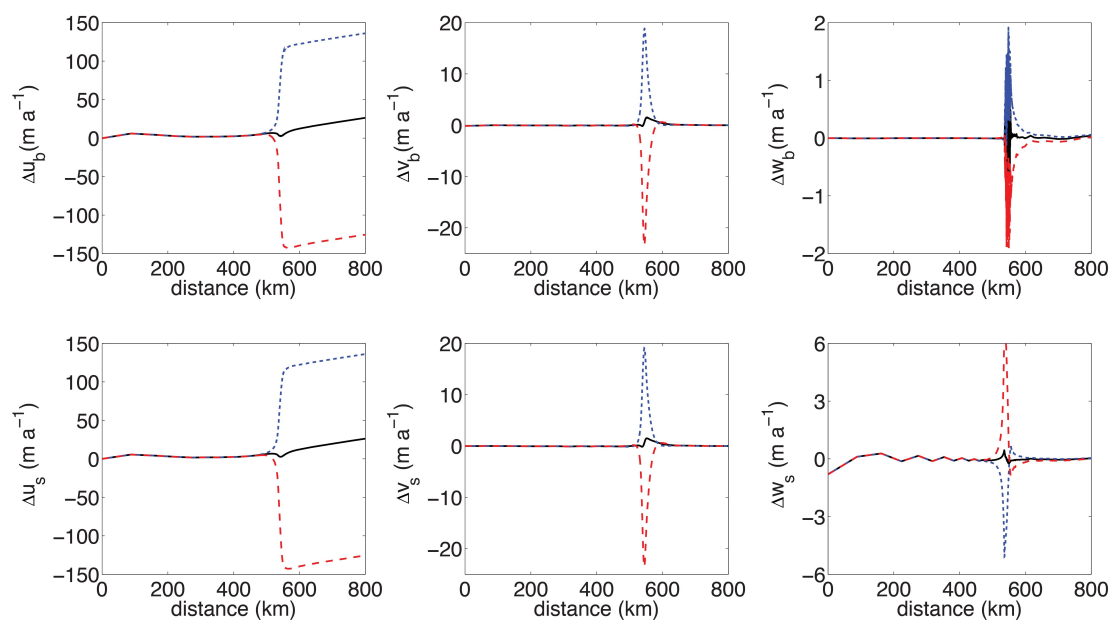


**Figure 3.** Comparisons of mean across-flow velocity differences for lower ( $\Delta u_b$ ,  $\Delta v_b$  and  $\Delta w_b$ ) and upper ( $\Delta u_s$ ,  $\Delta v_s$  and  $\Delta w_s$ ) surfaces along the  $x$  direction for FELIX-S and Elmer/Ice for the diagnostic experiment P75D. The blue-dotted, black-solid, and red-dashed lines denote the differences by subtracting Elmer/Ice LG, DI and FF values from FELIX-S values, respectively.

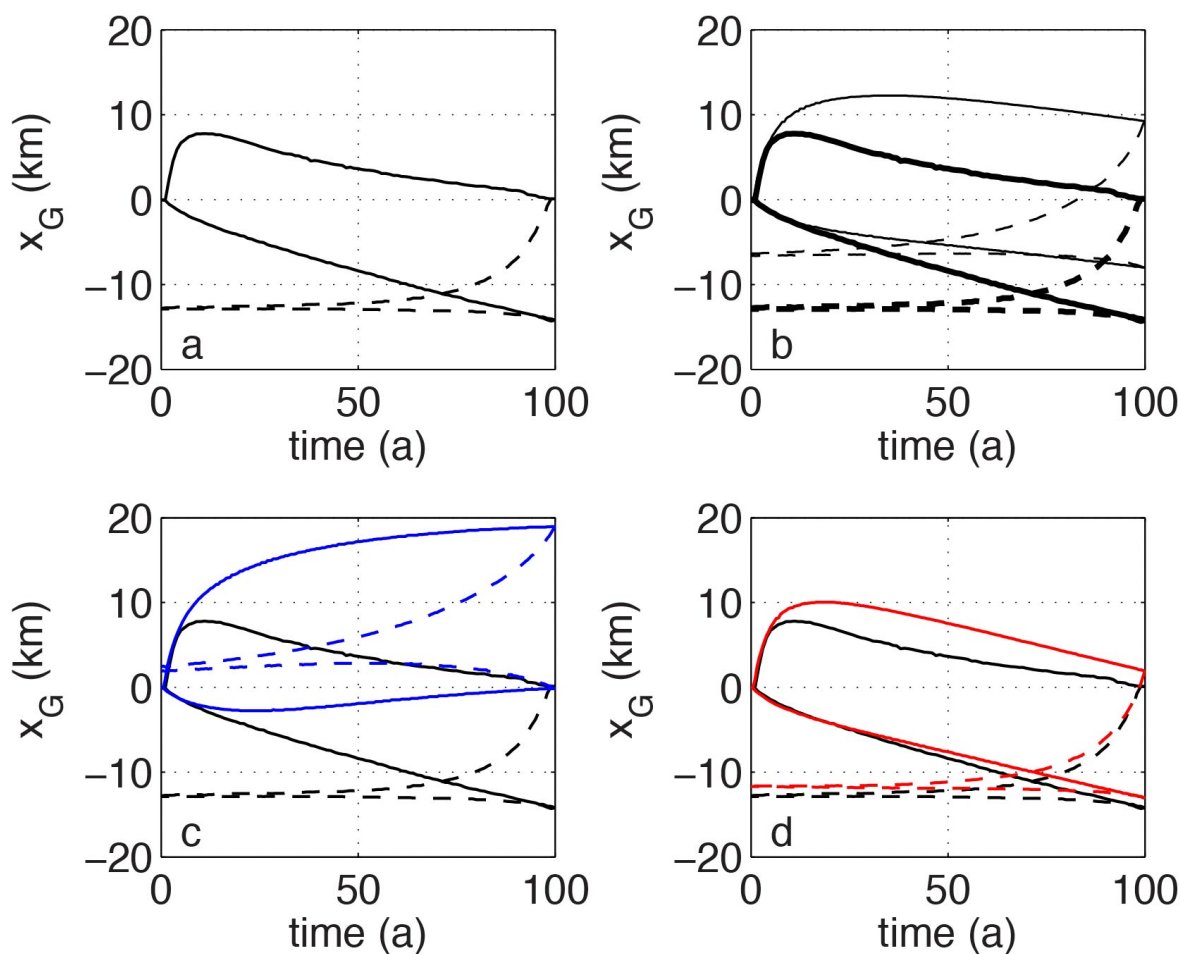


**Figure 4.** GL evolution on both the symmetry axis (upper curves) and free-slip boundary (lower curves) for the P75S (solid curves) and P75R (dashed curves) comparisons between FELIX-S (bold-black curve in b and black curves in a,c,d), and Elmer/Ice DI (b; thin-black curves), LG (c; blue curves) and FF (d; red curves). The number of elements along the  $y$  direction is 20 ( $\Delta y = 2500$  m).

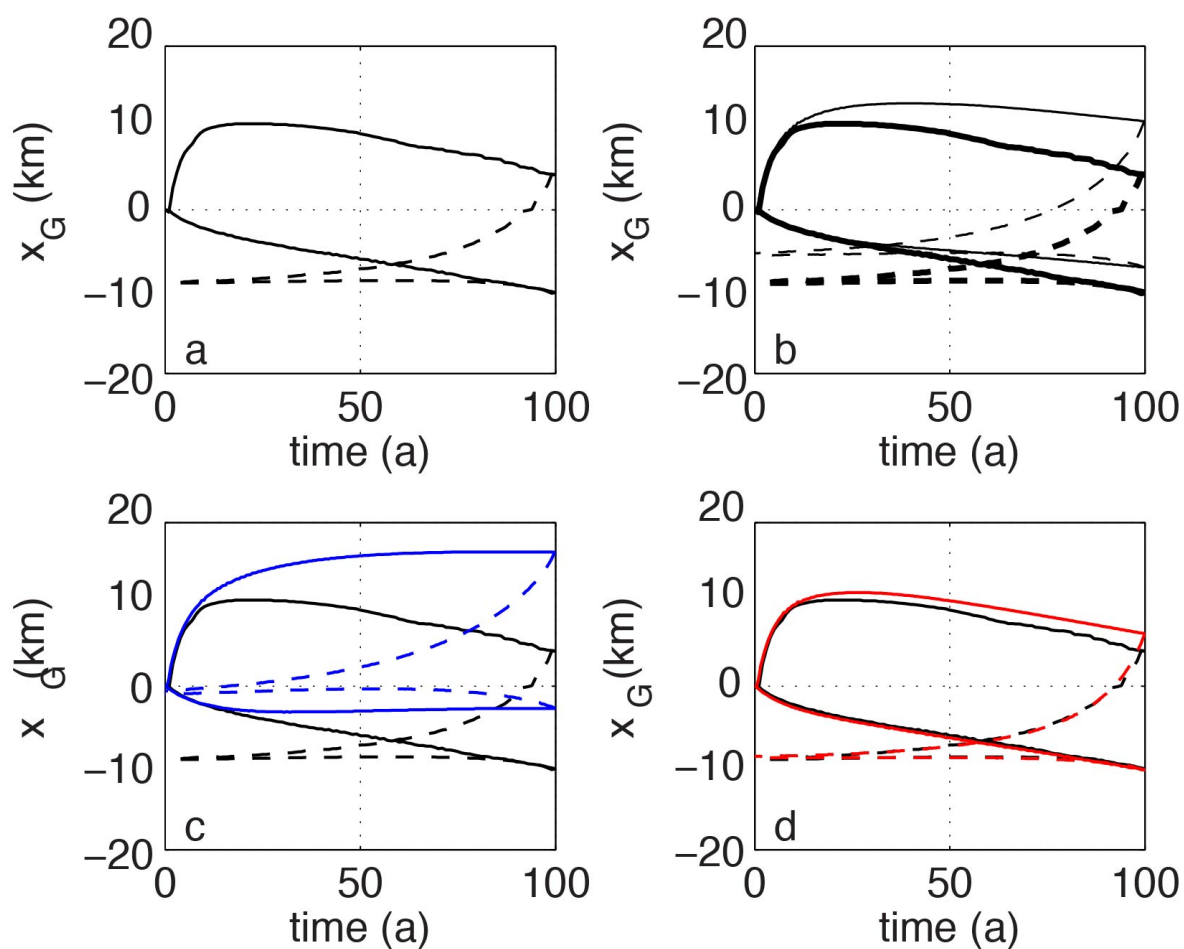


**Figure 5.** GL evolution on both the symmetry axis (upper curves) and free-slip boundary (lower curves) for the P75S (solid curves) and P75R (dashed curves) comparisons between FELIX-S (bold-black curve in b and black curves in a,c,d), and Elmer/Ice DI (b; thin-black curves), LG (c; blue curves) and FF (d; red curves). The number of elements along the  $y$  direction is 40 ( $\Delta y = 1250$  m).

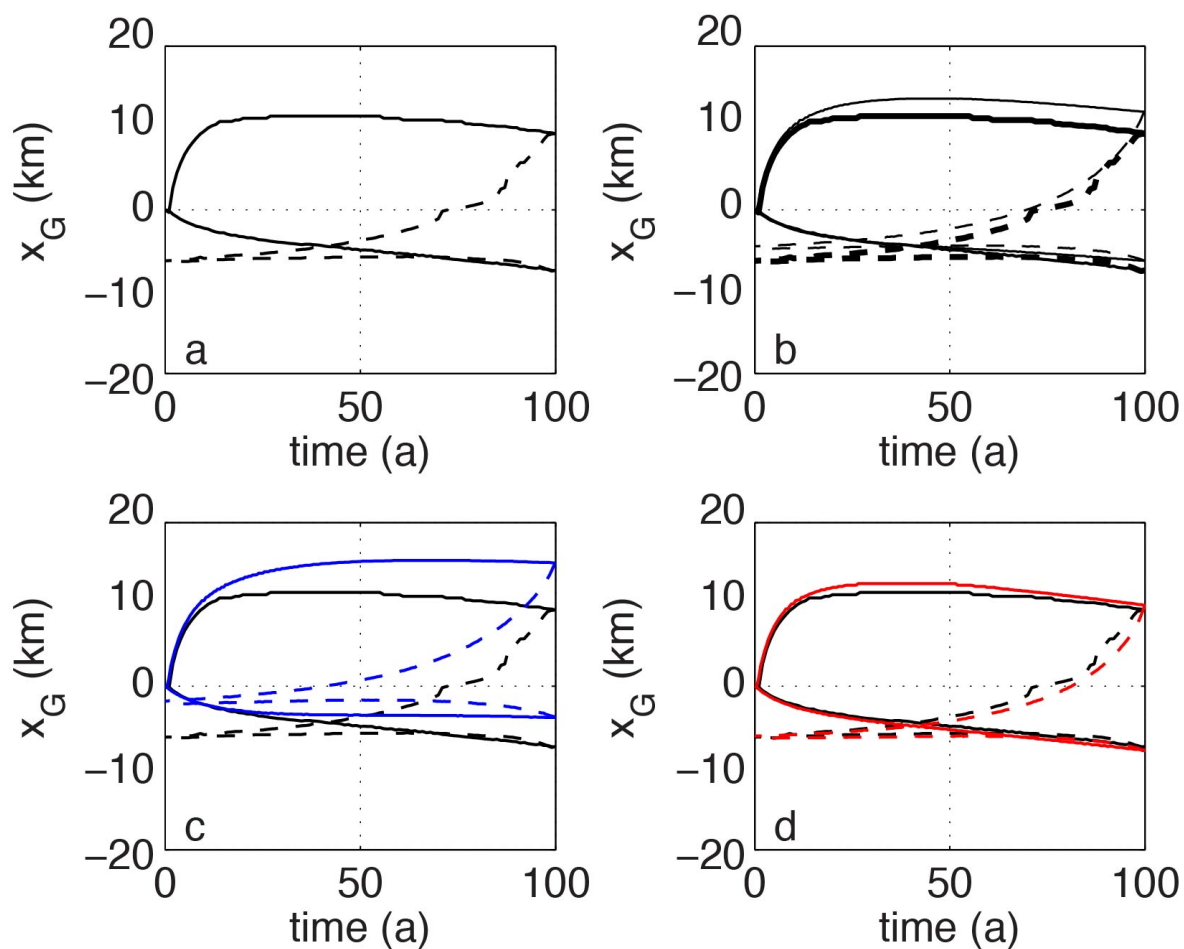


**Figure 6.** GL evolution on both the symmetry axis (upper curves) and free-slip boundary (lower curves) for the P75S (solid curves) and P75R (dashed curves) comparisons between FELIX-S (bold-black curve in b and black curves in a,c,d), and Elmer/Ice DI (b; thin-black curves), LG (c; blue curves) and FF (d; red curves). The number of elements along the  $y$  direction is 80 ( $\Delta y = 625$  m).

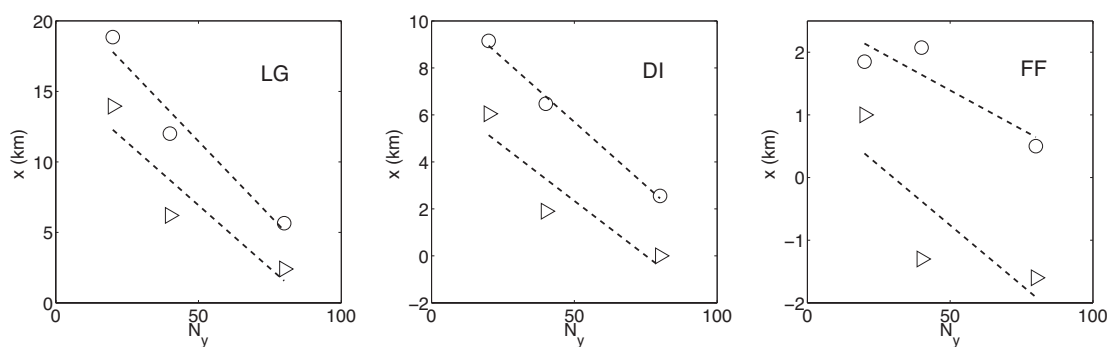


**Figure 7.** Absolute value of difference in final FELIX-S and Elmer/Ice (LG, DI and FF) GL positions at the centerline (circles) and margin (triangles) for the P75S experiment as a function of increasing across-flow ( $y$ ) resolution (resolution increases from 2500-625 m as  $N_y$  increases from 20-80). Dashed lines show the least-squares, linear fits to the data points, to emphasize approximate convergence of solutions with increasing mesh resolution.